JOURNAL OF THERMOPHYSICS AND HEAT TRANSFER
Vol. 24, No. 2, April–June 2010

Numerical Simulation of Melting in Porous Media via a Modified Temperature-Transforming Model

Piyasak Damronglerd* and Yuwen Zhang†
University of Missouri, Columbia, Missouri 65211

DOI: 10.2514/1.45420

A modified temperature-transforming model that considers the dependence of heat capacity on the fractions of a solid and a liquid in the mushy zone is employed to solve melting in porous media. Because natural convection only occurs in the liquid phase, the velocity of the phase change material in the solid region is set to zero by a ramped switch-off method. The convection in the liquid region is modeled using the Navier–Stokes equation with Darcy's term and Forchheimer's extension. The effect of natural convection is considered using the Boussinesq approximation. The results show that the temperature-transforming model with the heat capacity dependency are closer to experimental results with gallium as the temperature-transforming model and packed glass beads as the porous structure. The modified temperature-transforming model is then further used to study the melting of copper saturated in porous media and formed by sintered steel particles. The results show that melting is accelerated under a higher Rayleigh number, due to the stronger convection effect, and the melting is dominated by conduction for the case with a lower Darcy number.

Nomenclature

C	=	c^0/c_l
C_{sl}	=	c_s/c_l
C^0	=	equivalent heat capacity, $\mathrm{J}/(\mathrm{m}^3 \cdot \mathrm{K})$ [Eq. (7)]
c	=	specific heat, $\mathrm{J}/(\mathrm{kg} \cdot \mathrm{K})$
d_m	=	mean diameter of the sintered steel particles, m
g	=	gravitational acceleration, 9.8 $\mathrm{m/s}^2$
H	=	height of the enclosure, m
K	=	permeability, m^2
K_{eff}	=	dimensionless effective thermal conductivity, k_{eff}/k_l
K_{sl}	=	ratio of thermal conductivities, k_s/k_l
k	=	thermal conductivity, $\mathrm{W}/(\mathrm{m} \cdot \mathrm{K})$
L	=	latent heat, J/kg
L_x, L_y	=	number of nodes on the X and Y directions
P	=	dimensionless pressure, $(p + \rho_\infty g y)\mathrm{H}^2/\rho\nu_l\alpha_l$
Pr	=	Prandtl number, ν/α_l
Pr_l	=	Prandtl number of liquid, ν_l/α_l
p	=	pressure, $\mathrm{N/m}^2$
Ra	=	Rayleigh number, $g\beta H^3(T_h^0 - T_m^0)/\nu_l\alpha_l$
S	=	$S^0/c_l(T_h^0 - T_m^0)$
Sc	=	subcooling parameter, $(T_c^0 - T_m^0)/(T_h^0 - T_c^0)$
Ste	=	Stefan number, $c_l(T_h^0 - T_c^0)/h_{sl}$
S^0	=	source term in Eq. (4)
T	=	dimensionless temperature, $(T^0 - T_m^0)/(T_h^0 - T_c^0)$
T_i	=	dimensionless initial temperature
T^0	=	temperature, K
T_c^0	=	cold surface temperature, K
T_m^0	=	melting (or freezing) temperature, K
T_h^0	=	hot surface temperature, K
t	=	time, s
U, V	=	dimensionless velocities, uH/α_l, vH/α_l
u, v	=	velocities, m/s
X, Y	=	dimensionless coordinate directions, x/H, y/H
x, y	=	coordinate, m
α	=	thermal diffusivity, m^2/s
β	=	coefficient of volumetric thermal expansion, $1/\mathrm{K}$
ΔT	=	$\Delta T^0/(T_h^0 - T_m^0)$
ε	=	mass fraction of phase change materials in porous media
ζ	=	dimensionless permeability, K_ε/K_l
μ	=	dynamic viscosity, $\mathrm{kg}/(\mathrm{m} \cdot \mathrm{s})$
ν	=	kinematic viscosity, m^2/s
ρ	=	density, $\mathrm{kg/m}^3$, $\rho = \rho_\infty[1 - \beta(T^0 - T_m^0)]$
ρ_∞	=	reference density, $\mathrm{kg/m}^3$
τ	=	dimensionless time, $\alpha_l t/H^2$
φ	=	mass fraction of liquid phase in porous media
$2\Delta T^0$	=	phase change temperature range, K

Subscripts

i	=	initial value
l	=	liquid phase
m	=	mushy phase
s	=	solid phase

Received 13 May 2009; revision received 28 September 2009; accepted for publication 28 September 2009.

*Graduate Research Assistant, Department of Mechanical and Aerospace Engineering.

†Professor, Department of Mechanical and Aerospace Engineering. Associate Fellow AIAA.

I. Introduction

MELTING and solidification in porous media can find applications in a wide range of problems, including freezing and thawing of soil in a cold region, latent heat thermal energy storage, and selective laser sintering of metal powders. Although the early studies about phase change in porous media treated melting and solidification as conduction controlled, the effect of natural convection is often very important. Many numerical models for melting and solidification of various phase change materials (PCMs) have been developed. The numerical models can be divided into two groups [1]: deforming grid schemes and fixed grid schemes. Deforming grid schemes transform solid and liquid phases into fixed regions by using a coordinate transformation technique. The disadvantage of deforming grid schemes is that it requires a significant amount of computational time. On the contrary, the fixed grid schemes use one set of governing equations for the whole computational domain, including both liquid and solid phases, and the location of the solid–liquid interface is later determined from the temperature distribution. This simplicity makes the computation much faster than the deforming grid schemes, although it still provides reasonably accurate results [2]. There are two major methods in the fixed grid schemes: the enthalpy method and the equivalent heat capacity method. The

enthalpy method [3] can solve phase change that occurred at a single melting point (the solid and liquid phase are separated by a smooth interface) or occurred in a range of phase change temperatures (the solid and liquid phases are separated by a mushy zone that contains a mixture of solid and liquid phases). For the case in which phase change occurs at a single melting point, the enthalpy method has difficulty with temperature oscillation. The equivalent heat capacity method [4,5] assumes phase change occurs in a range of temperatures, which must be sufficiently large enough to obtain a converged solution.

Cao and Faghri [6] combined the advantages of both enthalpy and equivalent heat capacity methods, and they proposed a temperature-transforming model (TTM) that could also account for the effects of natural convection on melting and solidification. The TTM model was employed to analyze the performance of latent heat thermal energy storage systems [7,8]. Zhang and Faghri used TTM to study phase change in a microencapsulated PCM [9] and an externally finned tube [10]. Other research areas that TTM was extended into were the selective laser sintering of metal powder [11] and the laser drilling process [12,13].

Beckermann and Viskanta [14] propose a generalized model based on volume-averaged governing equations for melting and solidification in porous media that are applicable to the entire computational domain. This model includes the effect of inertia terms, which consequently allows nonslip conditions at the wall; this is a significant improvement over the Darcy's law that is valid only at very low velocity and assumes slip condition at the wall. The energy equation was obtained by combining the volume-averaged energy equation for the porous media and the change in the mean enthalpy equation (sensible and latent heat) for the fluid. Later, Chang and Yang [15] proved that Beckermann and Viskanta's model can handle even more complicated problems when the density of the PCM varied with the temperature. Chakraborty and Dutta proposed a generalized formulation for evaluation of latent heat functions in enthalpy-based macroscopic models for the convection–diffusion phase change process [16]. Pal et al. carried out an enthalpy-based simulation for the evolution of equiaxial dendritic growth in an undercooled melt of a pure substance [17]. In addition to the previously mentioned macroscopic models, Chatterjee and Chakraborty also developed an enthalpy-based lattice Boltzmann model for the diffusion dominated solid–liquid phase change [18], as well as a hybrid lattice Boltzmann model for the solid–liquid phase change in the presence of fluid flow [19]. DasGupta et al. proposed a homogenization-based upscaling as a superior technique over the conventional volume-averaging methodologies for effective property prediction in multiscale solidification melding [20].

The objective of this paper is to investigate the melting of copper saturated in sintered steel particles with the TTM and to improve the performance of the TTM by eliminating one important assumption. In the original TTM, the heat capacity within the range of the phase change temperature was assumed to be the average of that of a solid and a liquid, regardless of the liquid fraction in the mushy zone. Although this treatment could provide accurate results for the case that the heat capacity ratio of the PCM is close to unity ($\rho_s c_{ps} \approx \rho_\ell c_{p\ell}$), an alternative method that can consider the dependence of heat capacity on the fractions of a solid and a liquid in the mushy zone is necessary for the case that the heat capacity ratio is not close to 1. The heat capacity in the mushy zone is the weighted average of the heat capability of a liquid and a solid. The mass fraction of a liquid and a solid is a linear function of temperature in the mushy zone. The authors developed a modified TTM that considers heat capacity in the mushy zone as a linear function of solid and liquid mass fractions to solve natural convection-controlled melting in an enclosure heated from the side [21]. In this paper, the modified TTM will be extended to solve melting of copper saturated in porous media formed by sintered steel particles.

II. Modification of Temperature-Transforming Model

It is assumed that the flow is incompressible and the Boussinesq approximation is valid. The continuity and momentum equations for flow in porous media are

$$\frac{\partial u}{\partial x} + \frac{\partial v}{\partial y} = 0 \tag{1}$$

$$\frac{\rho_l}{\varphi_l}\frac{\partial u_l}{\partial t} + \frac{\rho_l}{\varphi_l^2}\left(u_l\frac{\partial u_l}{\partial x} + v_l\frac{\partial u_l}{\partial y}\right) = -\frac{\partial p}{\partial x} + \frac{\mu_l}{\varphi_l}\left(\frac{\partial^2 u_l}{\partial x^2} + \frac{\partial^2 u_l}{\partial y^2}\right) - u_l\left(\frac{\mu_l}{K} + \frac{\rho C}{\sqrt{K}}|u_l|\right) \tag{2}$$

$$\frac{\rho_l}{\varphi_l}\frac{\partial v_l}{\partial t} + \frac{\rho_l}{\varphi_l^2}\left(u_l\frac{\partial v_l}{\partial x} + v_l\frac{\partial v_l}{\partial y}\right) = -\frac{\partial p}{\partial y} + \frac{\mu_l}{\varphi_l}\left(\frac{\partial^2 v_l}{\partial x^2} + \frac{\partial^2 v_l}{\partial y^2}\right) - v_l\left(\frac{\mu_l}{K} + \frac{\rho C}{\sqrt{K}}|v_l|\right) - \rho g\beta(T^0 - T^0_{\text{ref}}) \tag{3}$$

where φ_l is the mass fraction of the liquid phase, and u_l is the average (pore) velocity of the liquid. The first- and second-order drag forces, namely Darcy's term and Forchheimer's extension, have been incorporated into Eqs. (2) and (3). Because the initial temperature is below the melting point, the entire domain is in a solid phase initially, so that the initial condition for Eqs. (1) and (3) is that the velocity is zero everywhere. The Boussinesq approximation is represented by the last term of Eq. (3). The superficial (Darcian) velocity is related to the pore velocity by

$$u = \varphi_l u_l \tag{4}$$

The permeability K can be obtained from the Kozeny–Carman equation [22]:

$$K(\varphi_l) = \frac{d_m \varphi_l^3}{175(1-\varphi_l)^2} \tag{5}$$

where d_m is the mean diameter of the sintered steel particles. The value of the inertia coefficient C in Forchheimer's extension has been measured experimentally by Ward [23], which was found to be 0.55 for many kinds of porous media.

The original TTM is based on the following assumptions: 1) solid–liquid phase change occurred within a range of temperatures; 2) the fluid flow in the liquid phase is an incompressible laminar flow with no viscous dissipation; 3) the change of thermophysical properties in the mushy region is linear; and 4) the thermophysical properties are constants in each phase but may differ among solid and liquid phases, whereas density is constant for all phases.

To use TTM in melting in porous media problems, the energy equation is transformed into a nonlinear equation similar to the method used in the temperature-based equivalent heat capacity methods. Assuming there is no density change during the phase change, and the liquid phase is incompressible, the original TTM expressed in a two-dimensional (2-D) Cartesian coordinate system is as follows:

$$\frac{\partial(C^0 T^*)}{\partial t} + \frac{\partial(C^0 u T^*)}{\partial x} + \frac{\partial(C^0 v T^*)}{\partial y} = \frac{\partial}{\partial x}\left(k\frac{\partial T^*}{\partial x}\right) + \frac{\partial}{\partial y}\left(k\frac{\partial T^*}{\partial y}\right) - \left[\frac{\partial(S^0)}{\partial t} + \frac{\partial(S^0 u)}{\partial x} + \frac{\partial(S^0 v)}{\partial y}\right] \tag{6}$$

where $T^* = T^0 - T^0_m$ is the scaled temperature, and the coefficients C^0 and S^0 in Eq. (6) are

$$C^0(T^0) = \begin{cases} (\rho c)_s, & T^0 < T^0_m - \Delta T^0 \\ (\rho c)_m + \frac{\rho h_{sl}}{2\Delta T^0}, & T^0_m - \Delta T^0 \le T^0 \le T^0_m + \Delta T^0 \\ (\rho c)_l, & T^0 > T^0_m + \Delta T^0 \end{cases} \tag{7}$$

$$S^0(T^0) = \begin{cases} (\rho c)_s \Delta T^0, & T^0 < T_m^0 - \Delta T^0 \\ (\rho c)_m \Delta T^0 + \frac{\rho h_{sl}}{2}, & T_m^0 - \Delta T^0 \le T^0 \le T_m^0 + \Delta T^0 \\ (\rho c)_s \Delta T^0 + \rho h_{sl}, & T^0 > T_m^0 + \Delta T^0 \end{cases} \quad (8)$$

and the thermal conductivity is

$$k(T^0) = \begin{cases} k_{s,\text{eff}}, & T^0 - T_m^0 < -\Delta T^0 \\ \frac{k_{l,\text{eff}} + k_{s,\text{eff}}}{2} + \frac{(k_{l,\text{eff}} - k_{s,\text{eff}})}{2\Delta T^0}(T^0 - T_m^0), & -\Delta T^0 \le T^0 - T_m^0 \le \Delta T^0 \\ k_{l,\text{eff}}, & T^0 - T_m^0 > \Delta T^0 \end{cases} \quad (9)$$

where $T^0 < T_m^0 - \Delta T^0$ corresponds to the solid phase, $T_m^0 - \Delta T^0 \le T^0 \le T_m^0 + \Delta T^0$ to the mushy zone, and $T^0 > T_m^0 + \Delta T^0$ to the liquid phase. Note that the mushy zone is the region where a liquid and a solid exist simultaneously. The effective conductivity of the liquid phase $k_{l,\text{eff}}$ should be calculated from

$$\frac{k_{l,\text{eff}}}{k_l} = (1-\alpha_0)\frac{\varepsilon f_0 + (1-\varepsilon f_0)k_p/k_l}{1-\varepsilon(1-f_0)+\varepsilon(1-f_0)k_p/k_l} + \alpha_0 \frac{2(1-\varepsilon)(k_p/k_l)^2 + (1+2\varepsilon)k_p/k_l}{(2+\varepsilon)k_p/k_l + 1 - \varphi_l} \quad (10)$$

where ε is the mass fraction of the PCM, k_l is the thermal conductivity for the liquid phase of the PCM, $f_0 = 0.8 + 0.1\varepsilon$, and

$$\log \alpha_0 = \begin{cases} -4.898\varepsilon & 0 \le \varepsilon \le 0.0827 \\ -0.405 - 3.154(\varepsilon - 0.0827) & 0.0827 \le \varepsilon \le 0.298 \\ -1.084 - 6.778(\varepsilon - 0.298) & 0.298 \le \varepsilon \le 0.580 \end{cases} \quad (11)$$

The effective thermal conductivity of the solid phase can be obtained by replacing k_l in Eq. (10) with k_s. The heat capacity in the mushy zone was assumed to be the mean average of those of the solid and liquid phases:

$$(\rho c)_m = \tfrac{1}{2}[(\rho c)_s + (\rho c)_l] \quad (12)$$

which is not a suitable assumption when the heat capacity ratio of the substance is not close to 1. To improve the TTM, it is proposed that the heat capacity is a function of the liquid fraction:

$$(\rho c)_m = (1-\varphi_l)(\rho c)_s + \varphi_l (\rho c)_l \quad (13)$$

where φ_l is the liquid fractions in the mushy zone, and the solid fraction is $1 - \varphi_l$. Because the mushy zone has a temperature from $T_m^0 - \Delta T^0$ to $T_m^0 + \Delta T^0$, the liquid fraction is a linear function of the temperature of the mushy zone by

$$\varphi_l = \frac{T^0 - T_m^0 + \Delta T^0}{2\Delta T^0}\varepsilon \quad (14)$$

The coefficients C^0 and S^0 for the energy equation of the modified TTM become

$$C^0(T^0) = \begin{cases} (\rho c)_s, & T^0 - T_m^0 < -\Delta T^0 \\ \frac{(\rho c)_l + (\rho c)_s}{2} + \frac{\rho h_{sl}}{2\Delta T^0} + \frac{(\rho c)_l - (\rho c)_s}{4}(T^0 - T_m^0), & -\Delta T^0 \le T^0 - T_m^0 \le \Delta T^0 \\ (\rho c)_l, & T^0 - T_m^0 > \Delta T^0 \end{cases} \quad (15)$$

$$S^0(T^0) = \begin{cases} (\rho c)_s \Delta T^0, & T^0 - T_m^0 < -\Delta T^0 \\ \frac{(\rho c)_l + 3(\rho c)_s}{4}\Delta T^0 + \frac{\rho h_{sl}}{2}, & -\Delta T^0 \le T^0 - T_m^0 \le \Delta T^0 \\ (\rho c)_s \Delta T^0 + \rho h_{sl}, & T^0 - T_m^0 > \Delta T^0 \end{cases} \quad (16)$$

and the thermal conductivity can still be obtained from Eq. (9).

Introducing the following nondimensional variables,

$$X = \frac{x}{H}, \quad Y = \frac{y}{H}, \quad U = u\frac{H}{\alpha_l}, \quad V = v\frac{H}{\alpha_l}, \quad \tau = \frac{\alpha_l t}{H^2}$$
$$T = \frac{T^0 - T_m^0}{T_h^0 - T_c^0}, \quad \Delta T = \frac{\Delta T^0}{T_h^0 - T_c^0}, \quad C_L = \frac{C^0}{(\rho c)_l}$$
$$C_P = \frac{(\rho c)_p}{(\rho c)_l}, \quad S = \frac{S^0}{(\rho c)_l (T_h^0 - T_c^0)}, \quad \zeta = \frac{K_\varepsilon}{K_l}$$
$$Da = \frac{K_\varepsilon}{L^2}, \quad Ste = \frac{c_l(T_h^0 - T_c^0)}{h_{sl}}, \quad C_{sl} = \frac{(\rho c)_s}{(\rho c)_l}$$
$$K_{\text{eff}} = \frac{k_{\text{eff}}}{k_l}, \quad K_{s,\text{eff}} = \frac{k_{s,\text{eff}}}{k_l}, \quad K_{l,\text{eff}} = \frac{k_{l,\text{eff}}}{k_l}$$
$$Ra = \frac{g\beta(T_h^0 - T_c^0)H^3}{\nu_l \alpha_l}, \quad P = \frac{H^2}{\rho \nu_l^2}(p + \rho g) \quad (17)$$

the governing equations can be nondimensionalized as

$$\frac{\partial U}{\partial X} + \frac{\partial V}{\partial Y} = 0 \quad (18)$$

$$\frac{1}{Pr_l}\left[\frac{1}{\varphi_l}\frac{\partial U}{\partial \tau} + \frac{1}{\varphi_l^2}\left(U\frac{\partial U}{\partial X} + V\frac{\partial U}{\partial Y}\right)\right] = -\frac{\partial P}{\partial X} + \frac{1}{\varphi_l}\left(\frac{\partial^2 U}{\partial X^2} + \frac{\partial^2 U}{\partial Y^2}\right) - U\left(\frac{\zeta}{Da} + \frac{C}{Pr_l}\sqrt{\frac{\zeta}{Da}}|U|\right) \quad (19)$$

$$\frac{1}{Pr_l}\left[\frac{1}{\varphi_l}\frac{\partial V}{\partial \tau} + \frac{1}{\varphi_l^2}\left(U\frac{\partial V}{\partial X} + V\frac{\partial V}{\partial Y}\right)\right] = -\frac{\partial P}{\partial Y} + \frac{1}{\varphi_l}\left(\frac{\partial^2 V}{\partial X^2} + \frac{\partial^2 V}{\partial Y^2}\right) - V\left(\frac{\zeta}{Da} + \frac{C}{Pr_l}\sqrt{\frac{\zeta}{Da}}|V|\right) + RaT \quad (20)$$

$$\frac{\partial (CT)}{\partial \tau} + \frac{\partial (UC_L T)}{\partial X} + \frac{\partial (VC_L T)}{\partial Y} = \frac{\partial}{\partial X}\left(\frac{K_{\text{eff}}}{Pr_l}\frac{\partial T}{\partial X}\right) + \frac{\partial}{\partial Y}\left(\frac{K_{\text{eff}}}{Pr_l}\frac{\partial T}{\partial Y}\right) - \left(\frac{\partial S}{\partial \tau} + \frac{\partial (US)}{\partial X} + \frac{\partial (VS)}{\partial Y}\right) \quad (21)$$

where

$$C = (1-\varepsilon)C_P + \varepsilon C_L \quad (22)$$

$$C_L = \begin{cases} C_{sl}, & T < -\Delta T \\ \frac{1+C_{sl}}{2} + \frac{1}{2Ste\Delta T} + \frac{1-C_{sl}}{4\Delta T}T, & -\Delta T \le T \le \Delta T \\ 1, & T > \Delta T \end{cases} \quad (23)$$

$$S = \begin{cases} C_{sl}\Delta T, & T < -\Delta T \\ \frac{1+3C_{sl}}{4}\Delta T + \frac{1}{2Ste}, & -\Delta T \le T \le \Delta T \\ C_{sl}\Delta T + \frac{1}{Ste}, & T > \Delta T \end{cases} \quad (24)$$

and the thermal conductivity is

$$K_{\text{eff}} = \begin{cases} K_{s,\text{eff}}, & T < -\Delta T \\ \frac{K_{l,\text{eff}} + K_{s,\text{eff}}}{2} + \frac{(K_{l,\text{eff}} - K_{s,\text{eff}})}{2\Delta T}T, & -\Delta T \le T \le \Delta T \\ K_{l,\text{eff}}, & T > \Delta T \end{cases} \quad (25)$$

The melting in porous media is now described by seven dimensionless parameters: Pr, Da, Ra, Ste, C_{sl}, C_p, and K_{eff}.

III. Numerical Procedures

The 2-D governing equations are discretized by applying a finite volume method [24], in which conservation laws are applied over finite-sized control volumes around grid points, and the governing equations are then integrated over the control volume. Staggered grid arrangement is used in discretization of the computational domain in momentum equations. The dimensionless conservation equations were numerically solved using the SIMPLE (semi-implicit method for pressure-linked equations) algorithm [24]. The power law scheme was used to approximate the combined convective and diffusive fluxes. The harmonic mean function was used for the diffusion coefficients, which ensure physically realistic results for abrupt changes in these coefficients.

To use the TTM in solid–liquid phase change problems, it is necessary to make sure that the velocity in the solid region is zero. In the liquid region, the velocity must be solved from the corresponding momentum and continuity equations. There are three widely used velocity correction methods [1]: the switch-off method (SOM), the source term method (STM), and the variable viscosity method (VVM). Voller [1] compared these three methods and concluded that SOM is the most stable method for phase change problem. Ma and Zhang [25] proposed two modified methods that can be used with TTM: the ramped SOM (RSOM) and the ramped STM (RSTM). These two methods were modified from the original SOM and the STM in order to eliminate discontinuity between the two phases. Because RSOM and RSTM give virtually the same results, this paper follows Ma and Zhang's recommendations and uses the RSOM for velocity treatment in a solid. The governing equations were solved throughout the physical domain, including the solid region, in which the velocities were controlled to zero by RSOM.

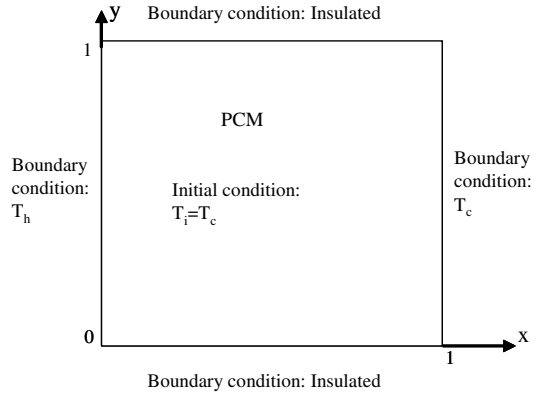

Fig. 1 Melting in a 2-D porous medium.

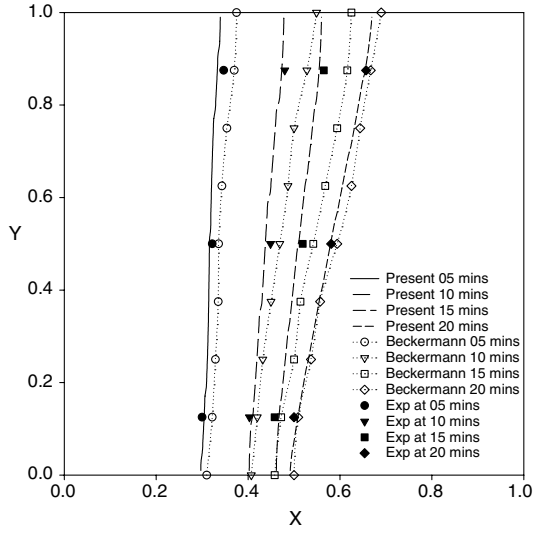

Fig. 2 Comparison of the locations of the melting fronts.

After many trials of 52×52, 82×82, 102×102, 82×52, and 102×52 grids in a computational domain, shown in Fig. 1, a grid of 102×52 nodal points and a dimensionless time step of $\tau = 1 \times 10^{-3}$ were used, because they give results at a minimal computational time. The lower grids of 52×52 and 82×52 could not give reasonable results, although the larger grid number did not significantly improve the results. Thus, the selected grid size and time step should be viewed as a compromise between accuracy and computational time. For each time step, the iterations were terminated when the relative dependent variables (values at each node divided by the maximum values) were less than the convergence criteria: 1×10^{-3} for the velocity components in the x and y directions, 1×10^{-6} for the temperature, and 1×10^{-7} for the maximum residual source of mass. Additional tests of the accuracy were performed for fluid flow in a rectangular enclosure without porous media, and good agreement was found.

IV. Results and Discussions

Melting inside a rectangular porous enclosure, as shown in Fig. 1, will be studied in this paper. Melting of gallium saturated in packed glass beads will be simulated first. The top and bottom walls are insulated, whereas the left and right walls are kept at a high constant dimensionless temperature of $T_h = 0.6$ and a low constant dimensionless temperature of $T_c = -0.4$, respectively. Both the PCM and the porous medium start with the initial temperatures T_c in all cases, which is above the fusion temperature $T_m = 0.0$. At time $t = 0$, the left wall temperature is increased to T_h, and melting starts from the left wall and progresses from left to right. The dimensionless parameters for the gallium–glass combination case are $Pr = 0.0208$, $Da = 1.37 \times 10^{-5}$, $Ra = 8.409 \times 10^5$, $Ste = 0.1241$, $C_{sl} = 0.89$, $C_p = 0.765$, $H = 1.0$, and $\varepsilon = 0.385$. The thermal conductivities used in the calculation of effective thermal conductivity are $k_s = 33.5$, $k_l = 32.0$, and $k_p = 1.4$ W/m · K, which give $K_{s,\text{eff}} = 0.384$ and $K_{l,\text{eff}} = 0.369$.

The modified TTM is validated by comparing it with the numerical and experimental results provided by Beckermann and Viskanta [14]. We used the same values for all of the parameters to make sure the only difference was the treatment of energy equation. Figure 2 shows the location of the melting front, which is identified by the fusion temperature, at different times. The results show the relatively weak effect of natural convection on the melting. This is expected, because the small Darcy number and the high effective thermal conductivity of the gallium–glass mixture suppress natural convection flow. At the beginning, conduction dominates the melting process (as represented by the interface), aligning almost vertically. Because the top and bottom of the enclosure is insulated, the problem is one-dimensional in the horizontal direction when melting is controlled by conduction. Therefore, the interface location is not a function of y, and this is the reason that vertical interface is seen. The interface becomes more inclined as the melting continues toward a steady state. This is an indication of natural convection showing its effects when the volume of fluid grows larger and the fluid circulation becomes stronger. The melting process reaches the steady state when heat received from the high-temperature wall on the left is equal to the heat released through the low-temperature wall on the right.

Both the modified TTM and the Beckermann and Viskanta model generally give very good prediction on the interface location when comparing them to the experimental results. However, the Beckmann and Viskanta model tends to overpredict the speed of the melting process, especially after the natural convection starts to show its effect, whereas the modified TTM can stay closer to the experimental results throughout the whole melting process. This could be the result of difference treatment to effective thermal conductivity and heat capacity in the mushy zone. Equation (10) gives effective thermal conductivity that is specialized for cases when the difference of thermal conductivities of the PCM and the porous media are very large, and it has a wider range of applications (see [26]). The modified TTM also treats the fluid fraction as a function of temperature, as

shown in Eq. (14). Consequently, the latent heat is included into the heat capacity calculation and has a direct link to the temperature (unlike in the combined energy equation, which treats latent heat as a separate source term). The modified TTM can predict the interface location with an error of less than 6% at any point and any time.

Figure 3 shows the temperature distribution at 5 and 15 min ($\tau = 1.8$ and 5.4), which confirms that the melting process starts as conduction dominated and then converts to convection dominated in later stages. The more subtle information that can be deducted from Fig. 3 is that, in the earlier stage, the temperature gradients in the liquid region are much higher than those in the solid region. If we focus on a very small control volume at the interface, keeping in mind that the thermal conductivities of solid and liquid gallium are very close (solid is only 5% higher than liquid), it is clear that heat transferring into the control volume is much higher than heat transferring out; hence melting occurs. As time goes on, temperature gradients in the liquid region decrease while gradients in the solid region increase, meaning the difference of heat going in and out of the control volume decreases. In other words, the heat responsible for the phase change decreases, so that the melting process consequently slows down. The isotherms are always perpendicular to the top and bottom walls because of the adiabatic conditions on them. The mushy zone, identified by $-\Delta T \leq T \leq \Delta T$, may start with a lower average temperature because a majority of the region is in the lower part of the temperature range. As the melting progresses, the average temperature of the mushy zone should increase. This indicates that the movement in the mushy zone is restricted, hence the effect of convection is minimal in the beginning, and then the restriction is gradually lifted when the average temperature increases. This mechanism contributes to, and once again confirms, the transition from a conduction- to convection-dominated melting process.

Figure 4 shows the approximate size of the mushy zone, which is identified by the temperature.

This temperature validation has established the reliability of the model, and so we further study the streamline to strengthen our confidence in the model. The streamline is defined as

$$\psi = \int U \, dY - \int V \, dX \tag{26}$$

Figure 5 shows streamlines at 5 and 15 min, at which the melting process is influenced by the typical natural convection. The fluid is heated by the left wall and rises toward the top wall. The hot fluid near the top wall moves faster and impinges upon the solid, causing it to melt faster. The melting rate decreases, because the fluid is cooled down as it descends along the interface and toward the bottom wall. It may also be seen that the streamline values increase as the flow develops, which illustrates increasing average velocity of the liquid flow. As a result, the curvature of the interface increases when convection is stronger. It should be pointed out that the temperature and streamline distributions at the 15 min mark are similar to those at a steady state (nearly 30 min), so that it can be concluded that the flowfield and temperature are almost fully developed at this stage.

The excellent agreement between the experimental results [14] and the numerical results from the modified TTM, as described previously, has led to a successful validation of the model. With full confidence that the modified TTM can give good results for melting in porous media problems, the model is then applied to another combination of materials. The combination consists of copper as the PCM and sintered steel particles as the porous medium. The dimensionless parameters for the copper–steel combination case are $Pr = 1.55 \times 10^{-3}$, $Da = 1.37 \times 10^{-5}$, $Ra = 1.28 \times 10^{6}$, $Ste = 0.0295$, $C_{sl} = 0.93$, $C_p = 1.09$, $H = 1.0$, and $\varepsilon = 0.385$. The thermal conductivities used in the calculation of effective thermal conductivity are $k_s = 352$, $k_l = 339$, and $k_p = 30$ W/m · K, which give $K_{s,\text{eff}} = 0.414$ and $K_{l,\text{eff}} = 0.402$. Figure 6 shows the melting fronts of copper at different times representing the melting process. The melting front is almost perpendicular to the top and bottom walls at the early stages. As time passes, there is little sign of the convection effects. The melting at the top section of the domain only progresses slightly faster than the bottom section, which shows the dominance of conduction in the melting process. This is because the effective thermal conductivity of the copper–steel mixture is roughly twice as high as that of the gallium–glass mixture, whereas the Rayleigh increases only in a small percentage. Such highly effective thermal

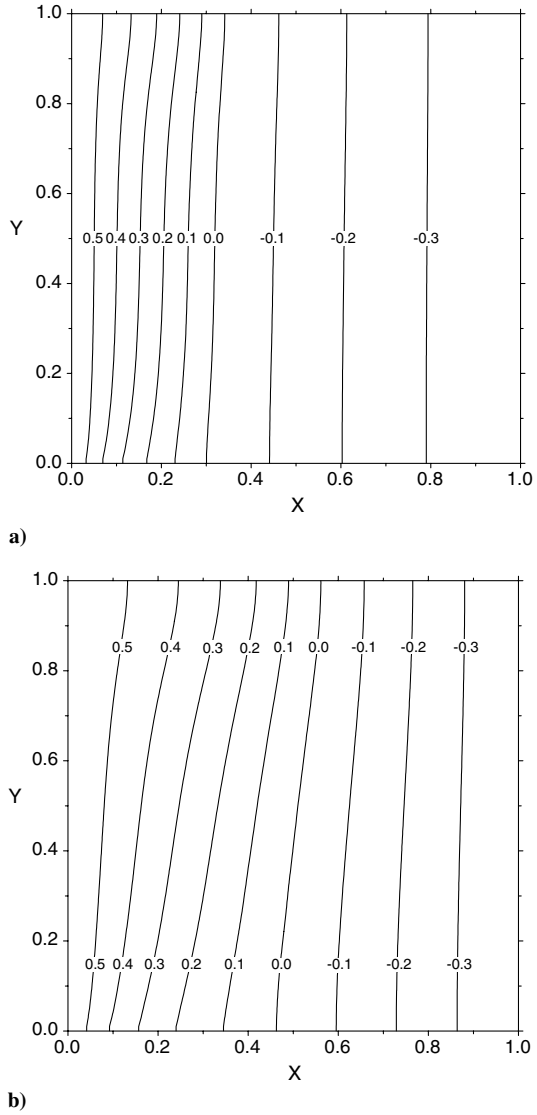

Fig. 3 Temperature distribution from the modified TTM at a) 5 and b) 15 min.

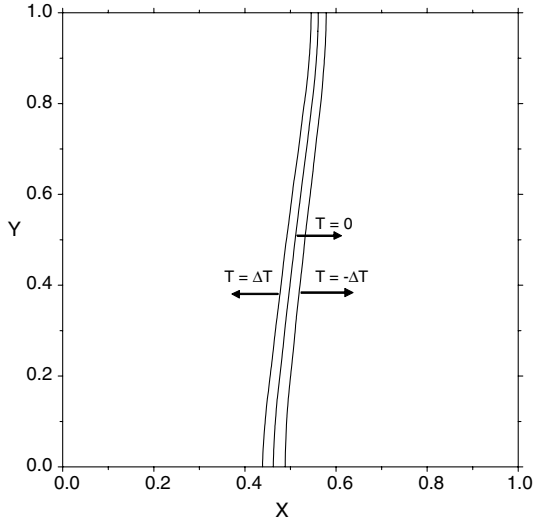

Fig. 4 The approximation of the mushy zone.

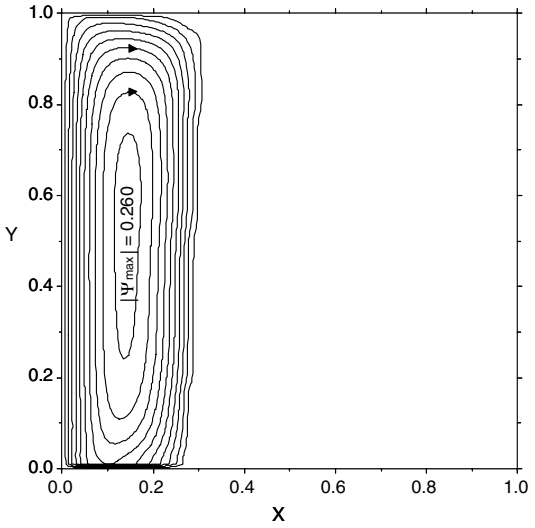

a)

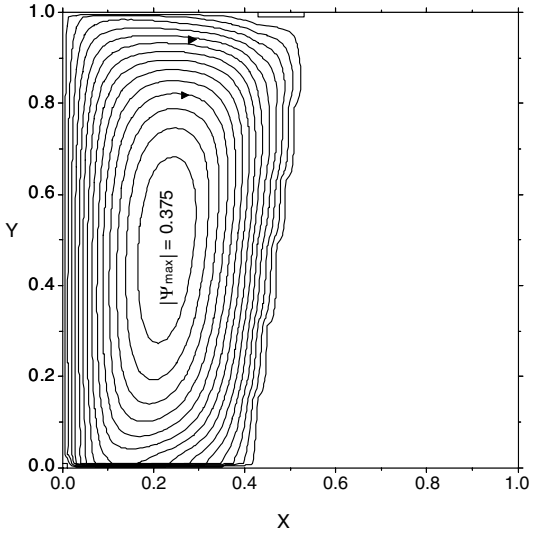

b)

Fig. 5 Streamlines from the modified TTM at a) 5 and b) 15 min.

conductivity tends to suppress the natural convection flow. Without the assistance of convection, the melting clearly progresses at a slower speed, hence it reaches the steady state at a lower volume of fluid. Because the right side of the enclosure is kept at a constant below the melting point. The melting process is essentially ceased at 20 min.

Figure 7 illustrates that natural convection still exists, even when conduction strongly dominates the melting process. However, the circulation is too slow to cause any significant effects. The fluid still rises up along the hot wall and falls down along the colder melting front. The impingement still causes the solid at the upper section to melt faster, even at this slow velocity. The temperature distribution in Fig. 8 confirms the conduction-dominated melting and the small effects of convection. The conduction-dominated melting is represented through the parallel temperature distribution, and the slightly inclined temperature line shows the effects of convection.

The changes occurring after we study different materials lead us to a question of what parameters actually control the melting process. In other words, it is interesting to know the parameters that dictate the types of melting processes. After a careful consideration of the parameters involved in the governing equations, there are three parameters that may be the controlling parameters: the Rayleigh number, Darcy's number, and the subcooling parameter. To study the effects of these parameters, all other settings were kept unchanged, and we only changed the focused parameter. The first parameter we studied was the Rayleigh number, as shown in Fig. 9.

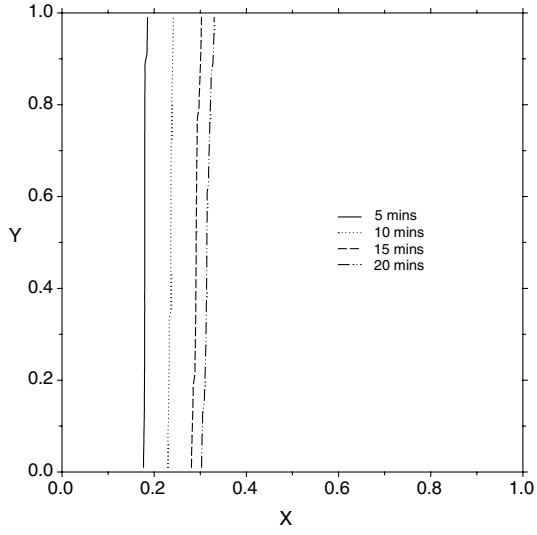

Fig. 6 Interface locations at different times for the copper–steel combination.

The case with the actual Rayleigh number was compared with two other cases: one with an order of magnitude lower and the other with an order higher. Figure 9 shows that the interface becomes more inclined when the Rayleigh number increases; this means the significance of convection increases with the Rayleigh number. The higher Rayleigh number equals the larger body force due to natural convection pushing the fluid to move faster, hence it increases the convection effects. Fast-moving fluid impinges on the melting front at a higher velocity and increases the melting rate near the top wall. Also, the high fluid velocity usually represents the high convective heat transfer coefficient, causing a higher overall melting rate; hence, the melting process is faster with a high Rayleigh number.

The effects of Darcy's number are then studied and shown in Fig. 10. The presence of convection also increases with a higher Darcy's number, and it only indirectly affects the conduction. The increasing Darcy's number results in larger pores inside the porous medium, which allows fluid to move with less restriction. When the fluid with the same Rayleigh number moves with smaller drags, it will move with a higher speed and consequently promote convection.

The last parameter is the subcooling parameter, shown in Fig. 11. The temperature at the hot wall remains the same for the three cases of subcooling: 0.2, 0.4, and 0.6. The results show that the melting front moves faster with a lower subcooling number, but the front shows very little change in convection. The interface moves faster because of the higher temperature gradient caused by the larger

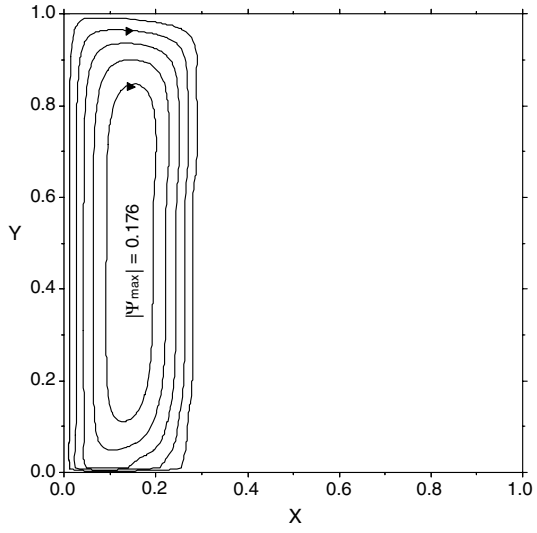

Fig. 7 Streamlines for the copper–steel combination at 20 min.

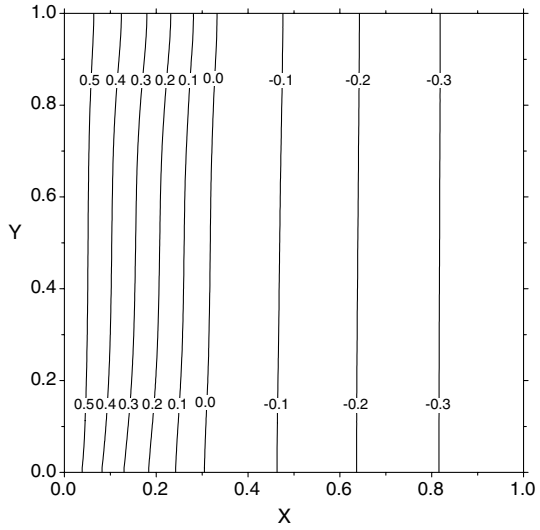

Fig. 8 Temperature distribution for the copper–steel combination at 20 min.

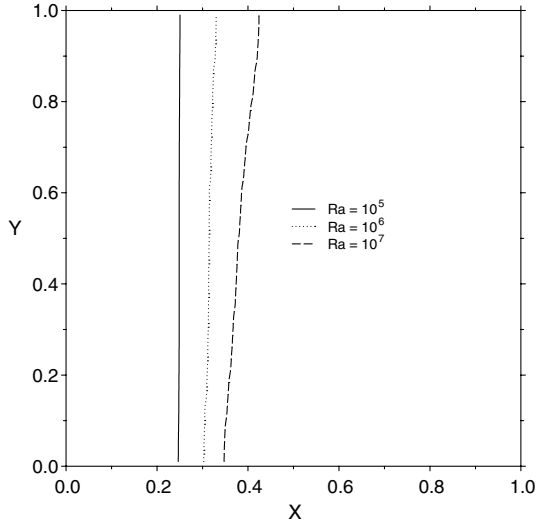

Fig. 9 Effects of the Rayleigh number on the melting process.

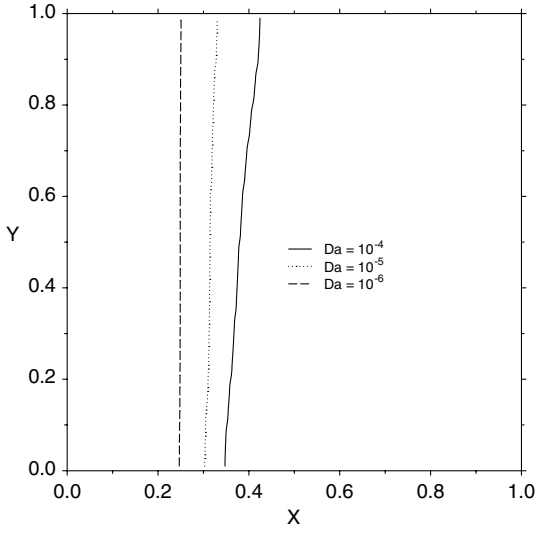

Fig. 10 Effects of Darcy's number on the melting process.

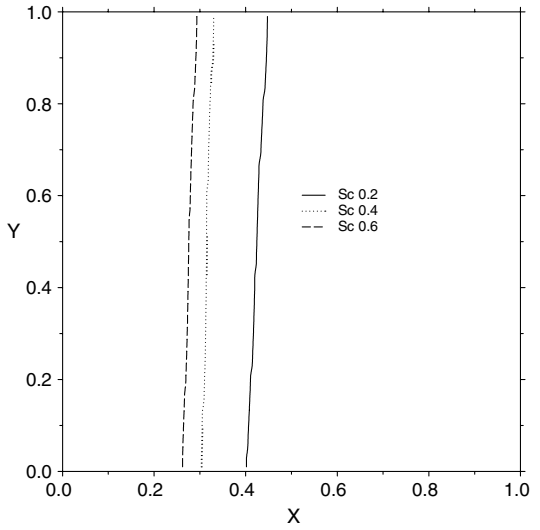

Fig. 11 Effects of the subcooling number on the melting process.

temperature difference between the two vertical walls, causing a higher rate of conduction heat transfer. Even though the temperature difference also appears in the Boussinesq approximation, and one would expect its effects on convection, the results clearly show that the effects are negligible in this case.

V. Conclusions

The TTM was modified to improve its performance in cases with a large heat capacity difference between the solid and liquid phases. The modified TTM clearly gave better predictions, whereas the existing approach tended to overpredict the speed of the melting process. Melting of copper saturated in sintered steel particles is then simulated using the improved TTM model. The results confirmed that higher effective thermal conductivity tends to suppress natural convection flow. The significance of the convection effects increases with the Rayleigh number and Darcy's number. Although increases of both numbers result in a faster fluid movement, they do so with different physical prospects. A large Rayleigh number increases the body force from natural convection, whereas a large Darcy's number reduces the drags on the fluid. Both numbers, however, only have a small effect on conduction, because they can only indirectly affect the temperature distribution. On the other hand, the subcooling parameter only affects the conduction because the larger temperature difference on both vertical walls results in a higher temperature gradient. Obviously, the modified TTM can be extended into many other research areas. It can be an excellent tool in other processes involving solid–liquid phase change, such as solidification and infiltration in porous media.

Acknowledgment

Support for this work by the U.S. Office of Naval Research, under grant number N00014-04-1-0303, is gratefully acknowledged.

References

[1] Voller, V. R., "An Overview of Numerical Methods for Solving Phase Change Problems," *Advances in Numerical Heat Transfer*, edited by W. J. Minkowycz, and E. M. Sparrow, Taylor and Francis, London, 1997.

[2] Sasaguchi, K., Ishihara, A., and Zhang, H., "Numerical Study on Utilization of Melting of Phase Change Material for Cooling of a Heated Surface at a Constant Rate," *Numerical Heat Transfer, Part A: Applications*, Vol. 29, No. 1, 1996, pp. 19–31. doi:10.1080/10407789608913776.

[3] Binet, B., and Lacroix, M., "Melting from Heat Sources Flush Mounted on a Conducting Vertical Wall," *International Journal of Numerical Methods for Heat and Fluid Flow*, Vol. 10, No. 3, 2000, pp. 286–306. doi:10.1108/09615530010318017

[4] Hsiao, J. S., "An Efficient Algorithm for Finite Difference Analysis of Heat Transfer with Melting and Solidification," American Society of

Mechanical Engineers Paper 84-WA/HT-42, 1984.

[5] Morgan, K., "A Numerical Analysis of Freezing and Melting with Convection," *Computer Methods in Applied Mechanics and Engineering*, Vol. 28, No. 3, 1981, pp. 275–284. doi:10.1016/0045-7825(81)90002-5

[6] Cao, Y., and Faghri, A., "Numerical Analysis of Phase Change Problems Including Natural Convection," *Journal of Heat Transfer*, Vol. 112, No. 3, 1990, pp. 812–816. doi:10.1115/1.2910466

[7] Cao, Y., and Faghri, A., "Performance Characteristics of a Thermal Energy Storage Module: A Transient PCM/Forced Convection Conjugate Analysis," *International Journal of Heat and Mass Transfer*, Vol. 34, No. 1, 1991, pp. 93–101. doi:10.1016/0017-9310(91)90177-G

[8] Cao, Y., Faghri, A., and Juhasz, A., "PCM/Forced Convection Conjugate Transient Analysis of Energy Storage Systems with Annular and Countercurrent Flows," *Journal of Heat Transfer*, Vol. 113, No. 1, 1991, pp. 37–42. doi:10.1115/1.2910548

[9] Zhang, Y., and Faghri, A., "Analysis of Forced Convection Heat Transfer in Microencapsulated Phase Change Material Suspensions," *Journal of Thermophysics and Heat Transfer*, Vol. 9, No. 4, 1995, pp. 727–732. doi:10.2514/3.731

[10] Zhang, Y., and Faghri, A., "Heat Transfer Enhancement in Latent Heat Thermal Energy Storage System by Using an External Radial Finned Tube," *Journal of Enhanced Heat Transfer*, Vol. 3, No. 2, 1996, pp. 119–127.

[11] Zhang, Y., Faghri, A., Buckley, C. W., and Bergman, T. L., "Three-Dimensional Sintering of Two-Component Metal Powders with Stationary and Moving Laser Beams," *Journal of Heat Transfer*, Vol. 122, No. 1, 2000, pp. 150–158. doi:10.1115/1.521445

[12] Ganesh, R. K., Faghri, A., and Hahn, Y., "A Generalized Thermal Modeling for Laser Drilling Process 1: Mathematical Modeling and Numerical Methodology," *International Journal of Heat and Mass Transfer*, Vol. 40, No. 14, 1997, pp. 3351–3360. doi:10.1016/S0017-9310(96)00368-7

[13] Ganesh, R. K., Faghri, A., and Hahn, Y., "A Generalized Thermal Modeling for Laser Drilling Process 2: Numerical Simulation and Results," *International Journal of Heat and Mass Transfer*, Vol. 40, No. 14, 1997, pp. 3361–3373. doi:10.1016/S0017-9310(96)00369-9

[14] Beckermann, C., and Viskanta, R., "Natural Convection Solid/Liquid Phase Change in Porous Media," *International Journal of Heat and Mass Transfer*, Vol. 31, No. 1, 1988, pp. 35–46. doi:10.1016/0017-9310(88)90220-7

[15] Chang, W. J., and Yang, D. F., "Natural Convection for the Melting of Ice in Porous Media in a Rectangular Enclosure," *International Journal of Heat and Mass Transfer*, Vol. 39, No. 11, 1996, pp. 2333–2348. doi:10.1016/0017-9310(95)00310-X

[16] Chakraborty, S., and Dutta, P., "A Generalized Formulation for Evaluation of Latent Heat Functions in Enthalpy-Based Macroscopic Models for Convection–Diffusion Phase Change Processes," *Metallurgical and Materials Transactions B: Process Metallurgy and Materials Processing Science*, Vol. 32, No. 3, 2001, pp. 562–564. doi:10.1007/s11663-001-0042-6

[17] Pal, D., Bhattacharya, J., Dutta, P., and Chakraborty, S., "An Enthalpy Model for Simulation of Dendritic Growth," *Numerical Heat Transfer, Part B: Fundamentals*, Vol. 50, No. 1, 2006, pp. 59–78. doi:10.1080/10407790500292366

[18] Chatterjee, D., and Chakraborty, S., "An Enthalpy-Based Lattice Boltzmann Model for Diffusion Dominated Solid–Liquid Phase Transformation," *Physics Letters A*, Vol. 341, Nos. 1–4, 2005, pp. 320–330. doi:10.1016/j.physleta.2005.04.080

[19] Chatterjee, D., and Chakraborty, S., "A Hybrid Lattice Boltzmann Model for Solid–Liquid Phase Transition in Presence of Fluid Flow," *Physics Letters A*, Vol. 351, Nos. 4–5, 2006, pp. 359–367. doi:10.1016/j.physleta.2005.11.014

[20] DasGupta, D., Basu, S., and Chakraborty, S., "Effective Property Predictions in Multi-Scale Solidification Modeling Using Homogenization Theory," *Physics Letters A*, Vol. 348, Nos. 3–6, 2006, pp. 386–396. doi:10.1016/j.physleta.2005.08.045

[21] Damronglerd, P., and Zhang, Y., "Modified Temperature-Transforming Model for Convection-Controlled Melting," *Journal of Thermophysics and Heat Transfer*, Vol. 21, No. 1, 2007, pp. 203–208. doi:10.2514/1.21529

[22] Kaviany, M., *Principles of Heat Transfer in Porous Media*, 2nd ed., Springer–Verlag, New York, 1995.

[23] Ward, J. C., "Turbulent Flow in Porous Media," *Journal of Hydraulic Engineering*, Vol. 90, No. HY5, 1964, pp. 1–12.

[24] Patankar, S. V., *Numerical Heat Transfer and Fluid Flow*, Hemisphere, Washington, D.C., 1980.

[25] Ma, Z., and Zhang, Y., "Solid Velocity Correction Schemes for a Temperature Transforming Model for Convection Phase Change," *International Journal of Numerical Methods for Heat and Fluid Flow*, Vol. 16, No. 2, 2006, pp. 204–225. doi:10.1108/09615530610644271

[26] Faghri, A., and Zhang, Y., *Transport Phenomena in Multiphase Systems*, Elsevier, New York, 2006.